J. Fluid Mech. (1970), *vol.* 41, *part* 2, *pp.* 259–281
Boeing Symposium on Turbulence

The turbulent boundary layer over a wall with progressive surface waves

By JAMES M. KENDALL

Jet Propulsion Laboratory, Pasadena, California 91103, U.S.A.

(Received 22 September 1969)

An experimental study of the interaction of a turbulent boundary layer with a wavy wall was conducted in a wind tunnel. A smooth neoprene rubber sheet comprising a portion of the floor of the tunnel was mechanically deformed into 12 sinusoidal waves which progressed upwind or down at controlled speed. The turbulent layer thickness was a little less than the wavelength. The mean velocity profile was linear on a semi-log plot over a substantial range of vertical height.

The wall pressure was observed to be asymmetrical about the wave profile, resulting in a pressure drag. Flow separation was not the cause of the drag. The drag was found to be larger than that predicted by the inviscid wave generation theory. The measurements indicate that the waves strongly modulate the turbulent structure. The phase of the turbulent stresses with respect to the waves varies with wave speed, indicating that the dynamical reaction time of the turbulence is not negligible in comparison with the wave period.

1. Introduction

The present experimental study of the response of a turbulent shear layer to a cyclic perturbation imposed from within the layer was motivated by an interest in the generation of water waves by wind. Interest is confined to that stage of the wave growth wherein the waves, having already been initiated in some unspecified manner, are of sufficient amplitude that the flow of air about the waves effects a transfer of momentum from the mean flow to the growing waves. Stewart (1967) has contended that most of the momentum given up by the wind appears as wave momentum, rather than as surface current momentum. Although the efficiency of the transfer processes is therefore high, the means by which the exchange occurs remains almost totally undetermined.

Two processes for momentum transfer are of probable importance. The first, involving the work done by the tangential shear stress upon the water surface motion, has been discussed by Stewart (1967) and Longuet-Higgins (1969). Longuet-Higgins showed that a cyclically variable stress is dynamically equivalent to a pressure force on the wave. Because neither the stress distribution nor the water surface motion are known in sufficient detail, an evaluation of the effectiveness of this mechanism has not been made.

The second process involves the pressure drag of the wave. Two mechanisms for the generation of a pressure component in phase with the wave slope have

Printed in Great Britain

received wide consideration. The first of these depends upon flow separation, but because separation probably occurs only over sharp-crested waves, the growth of small amplitude waves must have a different explanation. The other mechanism is contained in the well-known inviscid theory of Miles (1957, 1959). The theory has been amplified, extended, and explained in a number of articles including others by Miles, and by Benjamin (1959), Lighthill (1962) and Phillips (1966). Even though the omission of turbulence is probably serious, the inviscid theory retains a particular importance because it embodies a minimum of empiricism and is therefore least ambiguous, and because the mechanism of wave generation in a turbulent flow might retain certain features of the inviscid model. At present, no theory incorporates the major effects of turbulence in a satisfactory manner.

Experiments on the wind-wave interaction over the sea surface are being carried out by a number of investigators, and will eventually provide the ultimate understanding. Laboratory experimentation has been, and will continue to be, valuable. The number of experimental studies of the wave generation problem has increased rapidly in recent years. Unfortunately, none, including this one, is altogether adequate for evaluating even the relatively simple inviscid flow model.

Parameter	Sea	This experiment
Wavelength Reynolds number R_λ†	10^4–10^8	10^4–10^5
Stress coefficient C_τ‡	$\sim 2 \times 10^{-3}$	$\sim 4 \times 10^{-3}$
Wave amplitude $2a/\lambda$	0–0·14	0·06
Profile shape	Multi-component	Sinusoidal
Surface roughness	Variable	Smooth
Surface particle orbital motion	Forward circle	Retrograde ellipse

† Based respectively upon velocity at anemometer height, and upon free stream velocity.
‡ Throughout this work coefficients are based on the reference dynamic pressure and hence are twice the value which is based upon ρu^2.

TABLE 1

Most experiments have been limited to a determination of the wave-growth rate, or alternatively, the surface pressure, and the mean wind profile. Neither the growth nor the pressure are sensitive indicators of the details of the air motion. Recently, Karaki & Hsu (1968) and Stewart (1969) have measured the wave-producing stress $-\rho\overline{\tilde{u}\tilde{v}}$ over water waves in the laboratory. Here ρ is the air density and $\tilde{u}$ and $\tilde{v}$ are the streamwise and vertical components of the repetitive velocity perturbation. Although these results are clearly valuable, further study is needed.

The present experiment investigates the response of the turbulent flow structure to the perturbations imposed by a wavy wall, and attempts to examine further the evidence in favour of the inviscid wave generation mechanism. Aside from the surface pressure prediction, the assumptions and results of the inviscid theory to be tested here are: (1) the mean velocity u *versus* height y is represented by $u/u_1 = \ln y/z_0$, where u_1 is a reference velocity and z_0 is a length scale; (2) flow perturbations are sinusoidal; (3) a closed-streamline pattern

(vortex) rides atop each wave crest at the height of the critical layer, i.e. where $u = c$, c being the wave speed; (4) the stress $-\rho\overline{\tilde{u}\tilde{v}}$ is zero outside the critical layer, and takes a constant value equal to the force on the wave throughout the region between the critical layer and the wall.

Here, the flow over a mechanically generated wave train in a sheet of rubber was examined. The advantages with respect to water waves are: (1) the wavelength is independent of wave frequency; (2) the wave frequency can be chosen to be relatively high so that averages of fluctuating quantities over a prescribed number of wave cycles are attained more quickly; (3) the surface pressure and shear stress are relatively easy to measure; (4) the wave may travel upwind or down with equal ease.

A summary of some of the conditions of this experiment in contrast to those of the sea is given in table 1.

2. Equipment and techniques

Equipment

The experiment was conducted in a low turbulence wind tunnel in the speed range $u_\infty = 0$ to 16 m/sec. The constant-pressure test section was approximately 2 ft. square by 9 ft. long. The wavy wall comprised the latter 4 ft. of the floor of the test section. It was preceded by a five-foot smooth wood section, at the leading edge of which was a boundary-layer trip for the purpose of fixing the site of transition.

The surface of the wavy wall, figure 1, was composed of a $\frac{1}{4}$ in. thick neoprene rubber sheet which was constrained to form 12 sinusoidal waves, each with length $\lambda = 4{\cdot}00$ in. and trough-to-crest height $2a = 0{\cdot}25$ in. The surface smoothness was judged to be comparable to that of writing paper. The rubber was supported from underneath upon 49 ribs, each of which extended the two-foot width of the sheet, and was spaced at 1 in. intervals in the streamwise direction. The interval of arc length along the rubber was set equal to 1·02 in. to avoid a net stretching of the rubber. The ribs were attached to the rubber by a small fillet of rubber adhesive, forming a compliant flexure. Below each rib was a circular cam of 0·125 in. eccentricity. Each cam was positioned on a common camshaft, extending the length of the wall, with a successive phase difference of 90°. Rotation of the camshaft caused each rib to execute reciprocating vertical motion. The camshift was driven by a $\frac{1}{4}$ horsepower variable speed motor over the range 3–30 rev/sec in either direction. The corresponding wave speed was approximately $0{\cdot}30 < |c| < 3{\cdot}0$ m/sec.

The boundary conditions set by the wall are as follows. In addition to the dominant sinusoid, the wave profile possessed a distortion component with a wavelength equal to the rib spacing dimension and an amplitude of about 0·003 in. maximum. This distortion was discovered near the conclusion of the experiment. Wall slope measurements made early in the test programme did not disclose evidence of distortion, so that it is probable that the distortion developed with time. This slope measuring technique, described below, was also used to examine the possibility of inertial distortion of the rubber at high wave speeds.

Stroboscopically flashed light, triggered by the camshaft angular position, was employed. No variation of wall slope with wave speed was detected. The surface particle orbital motion resulting from the flexure of the rubber differed from the circular orbit of a deep water wave. Here, the orbit was an ellipse with a 3:1 vertical to horizontal axis ratio. The motion was retrograde with respect to that of a water wave. The upper surface of the rubber was strained in compression at the wave troughs, and in extension at the crests. The net strain over a wavelength was nominally zero.

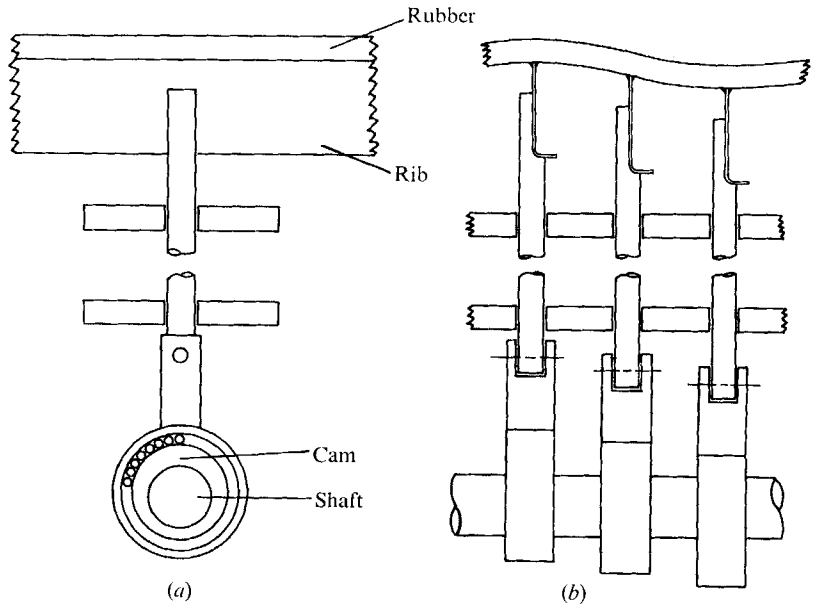

FIGURE 1. Wave machine. (*a*) Streamwise view. (*b*) Side view.

Pressure measuring techniques

The surface pressure was measured by means of 0·1 in. diameter orifices in the rubber sheet. The orifices were placed in four pairs along a line near the lateral centreline of the wave machine. The members of a pair were one-half wavelength apart in the streamwise direction, i.e. 2 in. The average distances of the orifice pairs behind the first rib of the machine were 6·5, 18·5, 30·5 and 42·5 in. These locations are subsequently referred to as stations 1–4. Measurement of the pressure by use of double orifices was necessitated by a sound pressure field generated by vibration of the wave machine and tunnel walls. Sound waves have long wavelengths at the frequencies considered here, i.e. below 30 Hz, whereas the pressure field of interest had a 4 in. wavelength. By adding the pressures of the two orifices with opposite polarity, the signal of interest was doubled, while the unwanted signal was cancelled.

Two techniques for connecting the orifices in the undulating wall to stationary pressure sensors were used. At stations 1–3, a length of 0·1 in. outside diameter metal tubing was placed in vertical alignment below each orifice, connected at the lower end to the sensor, and terminating at the upper end a little below

the level of the wave troughs. A short length of 0·1 in. inside diameter metal tubing encircled the first, and was sealed to the under side of the rubber wall, thereby forming a sliding seal in the fashion of a trombone. The air displaced by the relative motion between the wall and the tube produced an unwanted pressure, but this was estimated from loudspeaker theory to be negligible when $u_\infty \gtrsim 2c$.

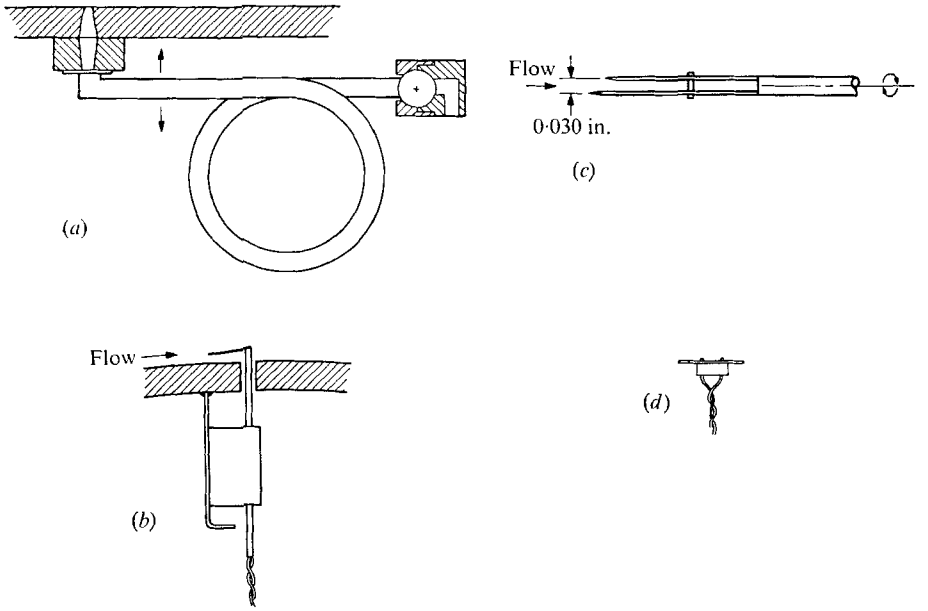

FIGURE 2. (*a*) Pressure duct, showing compensation loop and ball joint, streamwise view; (*b*) wall-mounted hot-wire probe attached to rib, side view; (*c*) inclined-wire probe, side view; (*d*) stress meter, streamwise view.

A more refined technique, shown in figure 2, was used at station 4, where most measurements were obtained. Essentially, a length of metal tubing formed a swinging arm between a stationary ball joint at one end, and the under side of the wall at the other. The loop served to cancel an unwanted pressure gradient generated by the acceleration of the duct. Simple considerations give an expression for the proper area of the loop. The accuracy of the cancellation was verified by a bench-test in which a replica of the system was oscillated in the horizontal plane, with liquid replacing the usual air for improved sensitivity. An unwanted pressure signal was also developed by the angular velocity excursions of the system, but these occurred at twice the principal frequency, and were rejected electronically.

The length of tubing connecting an orifice to its sensor was 5 in. for the first configuration, and 8 in. for the second. A correction for the pressure phase shift introduced by acoustic delay was incorporated in the data reduction.

The pressure was sensed by a matched pair of commercially manufactured strain gauge-type transducers, with 0·5 in. diameter diaphragms, and rated at 2·5 psi full scale. The cavity resonance of the transducer and tubing system

was relatively sharp, and located at 210 Hz, well above the range of interest. The transducer voltage was measured by a d.c. microvoltmeter for the case $c = 0$. For $c \neq 0$, a 10^4 gain preamplifier and a one-tenth octave bandpass sound analyzer were used for amplification, filtering and amplitude measurement.

The signal phase with respect to the wave pattern was measured by connecting the sinusoidal voltage output of the analyzer to one input of a phase meter. The reference input of the meter was driven by a square-wave voltage generated by the chopping of a light beam by a semi-circular shutter affixed to the camshaft of the wave machine. The phase of the wave at each orifice in relation to the camshaft rotation was determined by temporarily affixing fragments of mirrored glass to the wall beside each orifice. The reflexion angle of collimated light was analyzed to determine the principal axis of the wall slope. The phase shift of the preamp-analyzer combination was determined immediately prior to each pressure measurement by the substitution of an attenuated component of the light-chopper signal for the transducer signal.

The overall accuracy of the a.c. pressure technique was tested by measuring the pressure due to the passage of waves through still air. No boundary-layer effects are expected, so that the pressure perturbation, p_1, is known from linearized irrotational flow theory to be $Cp_1 = p_1/\frac{1}{2}\rho c^2 = -2ka \sin kx$. The measured amplitudes fell below this result with an error of 10 % for $c = 0{\cdot}6$ m/sec. The error decreased smoothly with increase of c to 3 % at $c = 3{\cdot}1$ m/sec. The phase angle, corrected for acoustic delay, showed no error greater than 5°.

Velocity measurements

The streamwise velocity at any height y is presumed to equal the sum of a steady component $u(y)$ and a fluctuating component u'. In turn, u' is the sum of a cyclically repetitive component $\tilde{u}$ and a random component u'_t. The vertical velocity is $\tilde{v} + v'_t$, defined similarly. The velocity components measured in the experiment are $u(y)$, $\tilde{u}$, $\tilde{v}$ and the double correlation terms $\langle u'v' \rangle$, $\langle \tilde{u}\tilde{v} \rangle$, $\langle u'_t v'_t \rangle$ and $\langle u'^2_t \rangle$. The brackets $\langle\ \rangle$ denote the time average of a cyclical variable prevailing at a particular wave phase. The quantity $\overline{\tilde{u}\tilde{v}}$ was obtained by averaging $\langle \tilde{u}\tilde{v} \rangle$ over an integral number of wave cycles.

All velocity measurements were obtained in the vicinity of station 4. Two hot-wire anemometer probes of conventional design were used for the measurement of the streamwise components u, $\tilde{u}$ and $\langle u'^2_t \rangle$. The first was mounted on a vertical traverse mechanism for surveying the region of the boundary layer extending from the wave crest to the outer edge. The second probe, shown in figure 2, was supported from a rib of the wave machine and thus followed the undulations of the wall at any preset height above the surface in the range 0 to 0·8 in.

The various quantities involving vertical velocity fluctuations were measured by means of an inclined wire probe, shown in figure 2, which was supported on the vertical traverse mechanism. This probe could be rotated about an axis set exactly parallel to the wave crest tangency line. Upon a half revolution, the inclination of the wire was precisely reversed without alteration of position.

A constant-temperature, linearized output, hot-wire set was used. The

frequency response was uniform to about 1·5 kHz, a value adequate for the present ratio of wind speed to boundary-layer thickness. Wire calibration and linearization were performed in the tunnel free stream. The voltage-velocity relationship for the two conventional wires was linear to within about 2 % of the free stream velocity. The inclined wire probe showed a similar accuracy for each inclination angle, and the response to variation of inclination angle was accurately linear for angles as large as $\pm 7°$, with no indication of departure beyond these limits.

The fluctuating voltage output of the inclined-wire probe in each of the two vertical-plane orientations was $e_1 = c_1 u' + c_2 v'$ and $e_2 = c_1 u' - c_2 v'$. The following quantities were determined:

$$\langle \tilde{v} \rangle = \frac{\langle \tilde{e}_1 \rangle - \langle \tilde{e}_2 \rangle}{2c_1}; \quad \langle \tilde{u}\tilde{v} \rangle = \frac{\langle \tilde{e}_1 \rangle^2 - \langle \tilde{e}_2 \rangle^2}{4c_1 c_2}; \quad \langle u'v' \rangle = \frac{\langle e_1^2 \rangle - \langle e_2^2 \rangle}{4c_1 c_2},$$

where the terms $\langle \tilde{e}_1 \rangle^2$ and $\langle \tilde{e}_2 \rangle^2$ indicate that the signal was first averaged, then squared, while $\langle e_1^2 \rangle$ and $\langle e_2^2 \rangle$ indicate that the signal was squared, then averaged. Two methods were used to determine $\langle u_t' v_t' \rangle$. The first employed the equality $\langle u_t' v_t' \rangle = \langle u'v' \rangle - \langle \tilde{u}\tilde{v} \rangle$. Because the sum of the four component voltage averages was small, accuracy was uncertain, and an independent technique was desirable. A method for recording and reproducing the components $\langle \tilde{e}_1 \rangle$ and $\langle \tilde{e}_2 \rangle$ in exact register with the total signal was developed. These were subtracted from the signal, thereby leaving only the turbulent components for analysis. The quantity $\langle u_t'^2 \rangle$ was determined similarly from the signal of a conventional probe.

The various voltage averages indicated in the formulas above were obtained by use of a 512 channel digital signal averaging instrument whose sweep was triggered by the light chopper on the wave machine. The number of wave cycles required to form a satisfactory average varied from a few hundred to several thousand, depending on the location of the probe in the boundary layer, and upon the particular quantity being averaged, with squared signals requiring the longer time. Signal squaring was accomplished by use of a wide-band analogue multiplier, with approximately 2 % accuracy. The hot-wire signal was a.c. coupled to the averaging and squaring instruments for the several double-velocity correlations because it is presumed that the mean value of each component independently is zero. Care was taken to avoid phase shift since the relative phase of the various harmonics of the signal is important.

Wall stress meter

The cyclic variation of the magnitude of the shear stress at the wall was determined by exploiting the analogy between that quantity and the heat transfer. A 'stress meter,' shown in figure 2, was constructed in the form of a modified hot-wire probe. An 0·08 in. length of hot-wire material was supported between two posts at a height of 0·005 in. above the surface of a $\frac{1}{4}$ in. square of 0·0005 in. thick metal foil. The height of the wire corresponds to a value of y^* less than 5 for the range of conditions tested. The foil was backed by a $\frac{1}{8}$ in. diameter stiffener disk in the area below the wire to prevent distortion of the foil. The meter was calibrated by temporarily affixing it to the flat floor of the tunnel ahead of the wavy wall. On the assumption that the stress coefficient is proportional to the

minus one-fifth power of the Reynolds number, the stress is proportional to $u_\infty^{1.8}$. The hot-wire linearizer controls were adjusted such that the output voltage reproduced this variation, following which the meter was remounted on the wavy wall in the vicinity of station 4. Its output was read on a d.c. voltmeter for the case $c = 0$, and by use of either the digital averager or sound analyzer and phase meter for the case $c \neq 0$.

3. Results

Format of presentation

In all cases, phase variation was obtained by moving the wave pattern past the flow-sensitive elements. Data were obtained with camshaft angle or with time as the independent variable. In each figure where such is required, a direction entitled 'Equivalent downwind co-ordinate' is indicated, and is the direction along which the distance of the sensor behind the wave crest increases. As an aid in distinguishing those hot-wire measurements obtained by use of the wall probe from those obtained by use of either traverse probe, the vertical location of the wall probe is denoted by y, while that of the traverse probes is denoted by y_c (except in figure 6). y_c is measured from the wave crest.

Pressure measurements

(*a*) *Measurements at* $c = 0$. Pressure data were obtained at station 4 for discrete settings of the camshaft angle, using d.c. measurement techniques. It is shown below that the results obtained at that station are approximately typical of those

u_∞, m/sec	$R_\lambda \times 10^{-4}$	C_{p_1}	ϕ_{p_1}, degrees	C_{D_p}
3·2	1·9	0·092	21·2	0·00323
5·5	3·3	0·102	15·6	0·00269
8·0	4·8	0·109	12·4	0·00229
10·6	6·4	0·121	9·8	0·00203

TABLE 2

obtained at all stations. The data, displayed in coefficient form in figure 3, indicate that the cyclic variation is approximately sinusoidal, and justify the subsequent disregard of the higher harmonic components in representing the pressure amplitude behaviour. The data were analyzed numerically to obtain the amplitude coefficient C_{p_1} and the phase angle ϕ_{p_1} of the fundamental frequency component for each value of u_∞. Positive values of ϕ_{p_1} indicate that the pressure is shifted downwind with respect to the surface depression profile. The pressure drag was calculated according to the relation

$$C_{D_p} = \frac{1}{\lambda}\int_0^\lambda C_p \frac{d\zeta}{dx}\, dx = \frac{C_{p_1}}{2}\, ka \sin \phi_{p_1},$$

where $ka = 0{\cdot}196$. The results are shown in table 2.

Two of the wave profiles tested by Motzfeld (1937) were sinusoidal, so that comparison with present results is appropriate. The amplitudes of the two models, I and II, were respectively $ka = 0{\cdot}157$ and $0{\cdot}314$; R_λ for both was $3{\cdot}3 \times 10^5$. The pressure distribution for model I only is included in figure 3, the range of

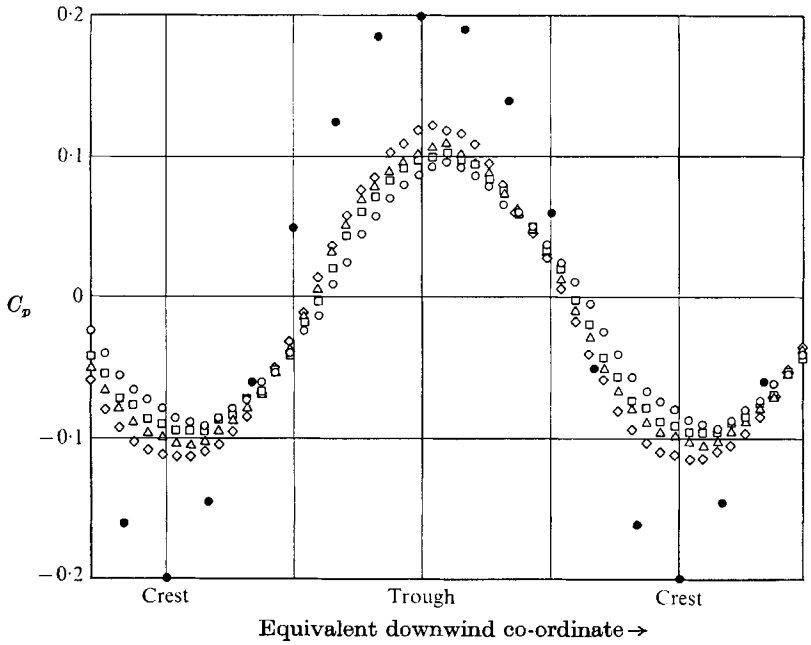

FIGURE 3. Pressure coefficient over a wavy wall: ○, □, △, ◇, u_∞ = 3·2, 5·5, 8·0, 10·6 m/sec respectively; ●, data of Motzfeld (1937) model I.

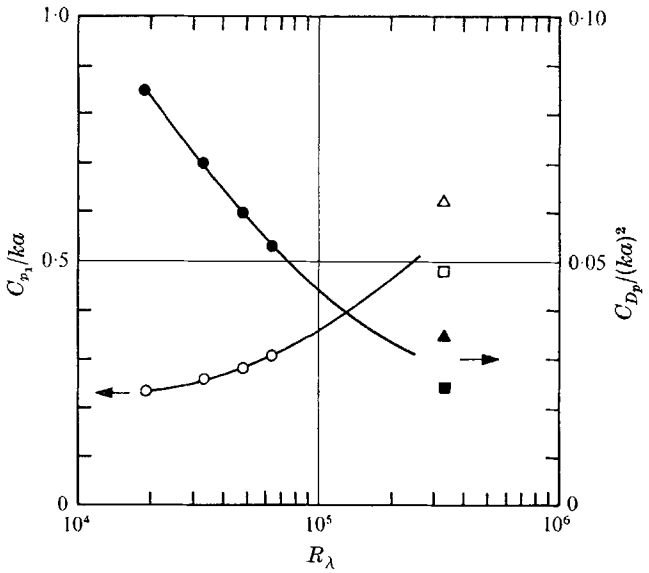

FIGURE 4. Reduced pressure coefficient (open symbols) and sheltering coefficient (solid symbols): ○, ●, present results; △, ▲, Motzfeld (1937) model I; □, ■, Motzfeld model II.

display being inadequate for inclusion of the model II results. Comparison based on the reduced amplitude $C_{p_1}/2ka$, and on the sheltering coefficient, $C_{D_p}/(ka)^2$, shown in figure 4 is more straightforward.

(*b*) *Streamwise development of pressure oscillations.* It is important to determine how quickly the flow attains an equilibrium behaviour after crossing the rather abrupt onset of surface waviness. For that reason, pressure measurements obtained at the four orifice stations were compared. The data were recorded by the use of a.c. techniques for the cases $c = 0{\cdot}3$, $0{\cdot}6$ and $2{\cdot}2$ m/sec, and for u_∞ ranging from approximately 3 to 12 m/sec. For each particular value of c and u_∞, the pressure coefficient C_{p_1} showed only modest station-to-station variation. The values at station 1 exceeded the approximately equal values prevailing at station 3 and station 4 by about 10–15 %, with the values at station 2 generally falling between those at stations 1 and 3. As will be demonstrated later, C_{p_1} was a sufficiently strong function of c/u_∞ that comparison with the results of table 2 is inappropriate.

The drag coefficient C_{D_p} perhaps offers a more meaningful basis of comparison of the station-to-station differences because it reflects the variation of both amplitude and phase values. Moreover, C_{D_p} is less sensitive to variation of c/u_∞, so that comparison with table 2 results is possible. The phase angle showed a somewhat wider station-to-station variation than did the amplitude, and was the more difficult quantity to measure. The unavoidable scatter of the data to some extent hinders the drawing of firm conclusions. For the cases $c = 0{\cdot}6$ and $2{\cdot}2$ m/sec, the C_{D_p} data of the several stations tended to reproduce the magnitude and the velocity dependence of the results given in table 2, and to show a station-to-station variation similar to that of C_{p_1} described above. For the case $c = 0{\cdot}3$ m/sec a stronger dependence on station location was found. C_{D_p} at station 1 was roughly double that at stations 3 and 4, where results consistent with table 2 were obtained. Station 2 values fell between station 1 and station 3 values.

To summarize, in no case did the pressure amplitude or phase results obtained at stations 3 and 4 differ significantly. Thus, over at least the latter half of the wall, the pressure results appear to depend only upon local conditions and not upon the history of the boundary condition.

(*c*) *Variation of pressure oscillations with wave speed.* The variation of C_{p_1}, ϕ_{p_1} and C_{D_p} with c/u_∞ at station 4 is shown in figure 5. Table 1 data are included. Three significant results stand out: (i) C_{p_1} varies faster than $(u_\infty - c)^2$. (ii) ϕ_{p_1} varies linearly with c/u_∞ in a range centred about $c/u_\infty = 0$, with the slope being nearly independent of R_λ. The acoustic delay correction incorporated in the displayed values of ϕ_{p_1} amounts to about 40 % of the linear phase variation for $u_\infty = 16$ m/sec, but is correspondingly less for lower values of u_∞. (iii) In the range $|c/u_\infty| \lesssim 0{\cdot}25$, the covariation of C_{p_1} and ϕ_{p_1} is such as to maintain the drag at values nearly equal to those of table 2 for $c = 0$.

The prediction of the inviscid theory of Miles (1959) may be compared with these results. The variables of the theory, α and β, are dependent upon the mean velocity profile parameters, which are shown below to vary to some extent with u_∞ and c. Thus an exact determination of α and β is tedious. For present purposes, it suffices to compute α and β from one typical profile, say, $u_\infty = 5{\cdot}5$ m/sec,

$c = 0$, recognizing that the prediction is only qualitatively correct for other profiles. According to table 3, presented later, the profile constants are $u_1/u_\infty = 0{\cdot}118$ and $kz_0 = 1{\cdot}6 \times 10^{-3}$. The following were used to compute the pressure behaviour.

$$\beta = \beta(ky_c); \quad ky_c = kz_0 e^{c/u_1}; \quad \alpha = -[(\beta/\pi ky_c) - \beta^2]^{\frac{1}{2}};$$

$$C_{p_1} = 2ka(\alpha^2 + \beta^2)^{\frac{1}{2}} \left(\frac{u_1}{u_\infty}\right)^2; \quad \phi_{p_1} = \tan^{-1}\beta/-\alpha; \quad C_{D_p} = (ka)^2\beta \left(\frac{u_1}{u_\infty}\right)^2.$$

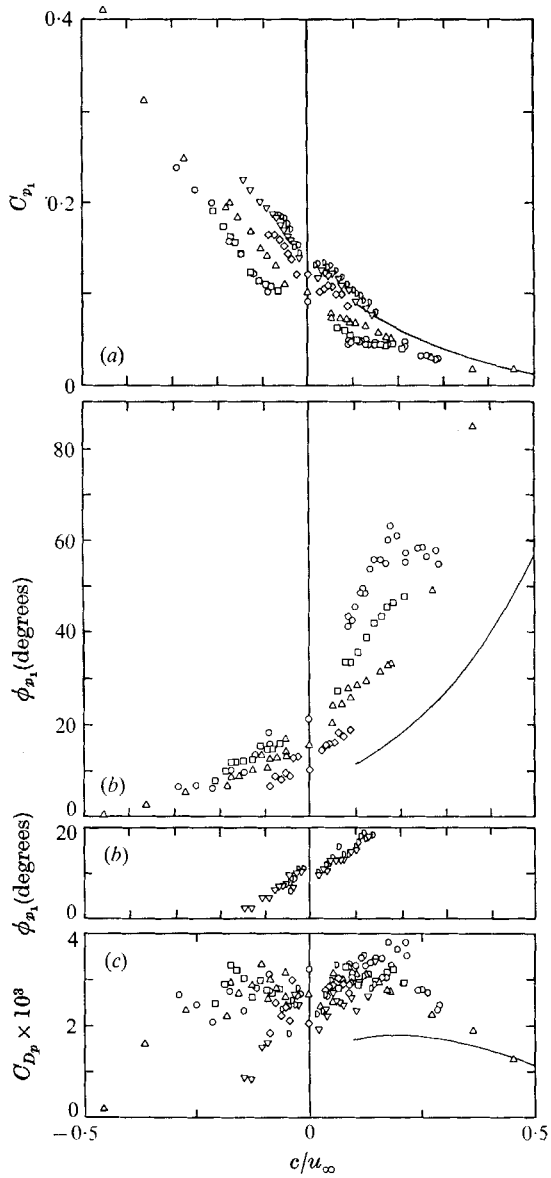

FIGURE 5. (*a*) Pressure amplitude coefficient; (*b*) phase angle of pressure; (*c*) pressure drag coefficient: ○, □, △, ◇, ▽, ▷, u_∞ = 3·2, 4·4, 5·5, 10·6, 13·2, 16·0 m/sec respectively; ——, inviscid theory.

The results are included in figure 5. Note that the comparison is only appropriate for the case where the critical layer lies outside the laminar sublayer edge, $c/u_\infty \gtrsim 0{\cdot}4$.

Velocity measurements

(*a*) *Mean velocity.* Three profiles of velocity *versus* the vertical co-ordinate are shown in figure 6. The curves labelled 'max' and 'min' were measured for $c = 0$ at stations 15° upwind and 125° downwind of the wave crest, respectively, and represent the limits of excursion of the cyclic velocity perturbation. The curve labelled 'mean' represents the mean value of the velocity over the wave cycle. In this figure, the values of y indicated for the traverse-mounted probe

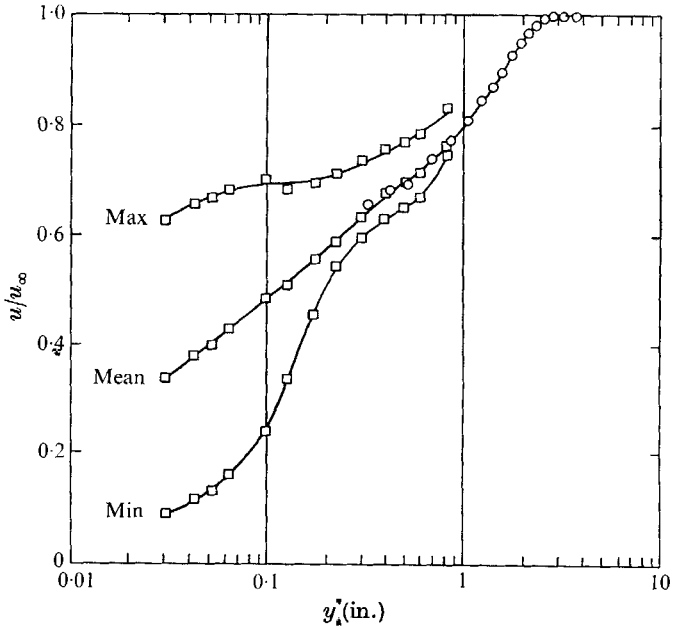

FIGURE 6. Mean velocity profile, $u_\infty = 5{\cdot}5$ m/sec, $c = 0$: ○, traverse probe; □, wall probe.

are measured from the mean surface elevation and are consistent with those of the wall probe. Mean profiles measured at two other values of u_∞ closely resembled that of figure 6, except that the edge of the sublayer was more apparent at the lowest value of u_∞. The straight-line portions of the profiles may be represented by $u/u_1 = \ln(y/z_0)$. Table 3 gives values of u_1, z_0, and the friction coefficient, C_f, for the three values of u_∞. Here $C_f = 2(u_*/u_\infty)^2$, where u_* is taken to be $0{\cdot}4\,u_1$.

The variation of the mean velocity profile with wave speed was examined in some detail. It was found that the effect of varying c was to produce an approximately parallel displacement of the straight-line portion of the profile, i.e. to alter z_0, but not u_1. Data obtained by the traverse-mounted and wall-mounted probes exhibited similar results, thus tending to eliminate vertical velocity sensitivity as a possible cause of the variation. The velocity shift $\Delta u/u_\infty$, where Δu is referred to the profile at $c = 0$, was dependent upon c/u_∞ and approximately independent of u_∞. For $c/u_\infty < 0{\cdot}1$, the slope of $\Delta u/u_\infty$ with c/u_∞ was negative,

producing a value $\Delta u/u_\infty$ of about 0·15 at $c/u_\infty = -1$. For $0{\cdot}1 < c/u_\infty < 0{\cdot}8$, the slope was positive, resulting in $\Delta u/u_\infty = 0{\cdot}15$ at $c/u_\infty = 0{\cdot}8$. For $c/u_\infty > 0{\cdot}8$, the slope tended toward negative values. In brief, increasing $|c/u_\infty|$ toward unity, the limit of observation, increased the velocity in the boundary layer 0·15 u_∞ at most.

u_∞, m/sec	u_1/u_∞	kz_0	C_f
2·15	0·13	0·0032	0·0054
5·5	0·118	0·0016	0·0045
10·6	0·085	0·0004	0·0023

TABLE 3

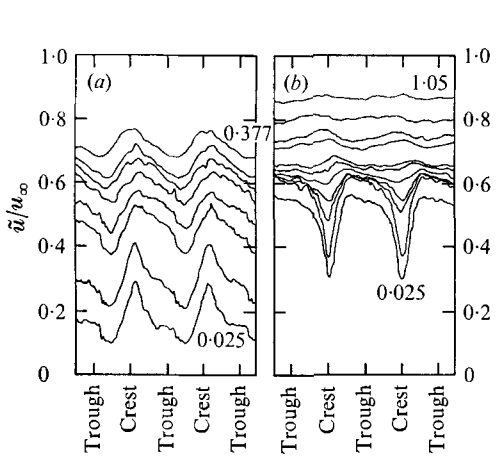

FIGURE 7

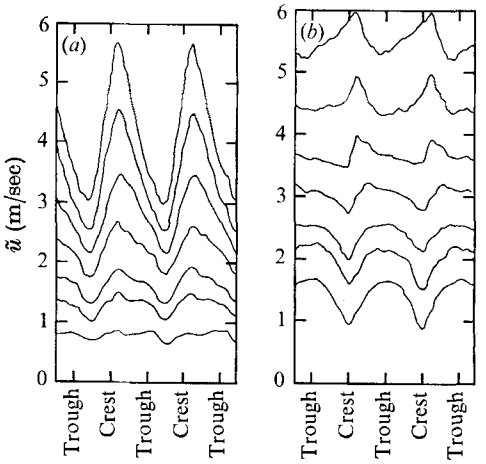

FIGURE 8

FIGURE 7. $\tilde{u}$ fluctuation, including mean velocity, $u_\infty = 5{\cdot}5$ m/sec, $c = 3{\cdot}0$ m/sec: (*a*) wall probe, $y = 0{\cdot}025$, 0·032, 0·050, 0·072, 0·116, 0·166, 0·225 and 0·377 inches above wall; (*b*) traverse probe, y_c = same as (*a*), plus 0·482, 0·75 and 1·05, all values measured in inches above crest.

FIGURE 8. $\tilde{u}$ fluctuation including mean velocity, $c = 3{\cdot}0$ m/sec; (*a*) wall probe, $y = 0{\cdot}052$ in. above wall, $u_\infty = 3{\cdot}0$, 3·8, 4·4, 5·5, 6·8, 8·0 and 9·3 m/sec; (*b*) traverse probe, $y_c = 0{\cdot}080$ in. above crest, u_∞ same as (*a*).

(*b*) $\tilde{u}$ *results.* Measurements of $\tilde{u}$ were obtained by both the wall-mounted and traverse-mounted probes for values of y ranging approximately from the edge of the laminar sublayer to half the boundary-layer thickness, and for c/u_∞ ranging from 0·11 to 0·64. As a general result, the records obtained by the traverse-mounted probe showed such diversity of wave-form and complexity of progression with vertical location that it is impractical to present all possibilities. Representation is therefore limited to the display of the y variation of the wave-form at one value of c/u_∞, figure 7, and to the variation with c/u_∞ at constant y, figure 8.

Several conclusions may be drawn from these and the other measurements.

(i) Near the wall, the waveform observed by neither probe is sinusoidal.

(ii) Near the wall, the waveforms recorded by the two probes differ vastly because the variation of velocity along the phase of the wave is less than the vertical variation occurring within a distance equal to the divergence of the two probe paths, i.e. the wave amplitude.

(iii) The phase of the fundamental frequency component of $\tilde{u}$ recorded by the traverse probe is highly variable with y for the same reason the waveform varies. The phase of that quantity recorded by the wall probe shows little variation with either c/u_∞ or y. On the average, it is 30–50° upwind of the phase of the wall elevation. Comparison of phase results with theory will therefore require a judgement as to which result is more appropriate.

(iv) In no case is a phase reversal of the waveform with variation of y observed at the location of the critical layer. There is no vortex pattern fixed with respect to the wall.

(v) The amplitude of the $\tilde{u}$ waveform diminishes with c/u_∞. For such case that the critical layer lies outside the laminar sublayer, i.e. $c/u_\infty \lesssim 0{\cdot}4$, the amplitude of $\tilde{u}$ is everywhere small compared to that of the turbulent fluctuation. The motion is highly disorganized, and the absence of a permanent vortex system is not surprising. For the conditions of figure 7, $c/u_\infty = 0{\cdot}55$, the peak-to-peak value of $\tilde{u}$ recorded by the wall probe at the average height of the critical layer, 0·1 in., is about $0{\cdot}1\ u_\infty$, whereas the turbulent fluctuations show excursions of about $0{\cdot}4\ u_\infty$. The $\tilde{u}$ contribution is not perceptible to the eye in a photograph of the u' signal there.

(vi) The amplitude of $\tilde{u}$ diminishes rapidly with y. Thus the oscillatory flow studied in this experiment should closely resemble that in a flow for which the logarithmic profile is of infinite extent.

(vii) The height of the critical layer above the wall, determined from figure 7, is found to vary along the phase of the wave from a minimum of 0·08 in. 90° upwind of the crest to a maximum of 0·12 in. 90° downwind of the crest. The layer imitates the profile of the wave, but is displaced downwind about 20°.

(*c*) $\tilde{v}$ *results.* Owing to the distortion of the profile of wall elevation mentioned in §2, the amplitude and waveform of $\tilde{v}$, but not $\tilde{u}$, were dependent upon the x location of the probe with respect to the ribs of the wave machine. The variability of $\tilde{v}$ with x was found to depend upon c/u_∞. For $c/u_\infty \lesssim 0{\cdot}3$, it was not significant, while at $c/u_\infty = 0{\cdot}65$ the peak amplitude varied cyclically along x by a factor of two. This importance of wave profile distortion bears implication for laboratory water-wave experiments as well. Any non-permanence of the waveform, whether due to reflexion or to higher harmonic components of waves excited by a wavemaker, can affect measured values of $\tilde{v}$ and $\tilde{u}\tilde{v}$.

The measurements were carried out at several heights above the wall and at a variety of positive wave-to-wind speed ratios. Most data were obtained at $u_\infty = 5{\cdot}5$ m/sec. The x station of the probe for the results discussed here was midway between two adjacent locations where the waveform amplitude assumed maximum and minimum values at high c/u_∞. The results are therefore approximately equal to the average prevailing along the wall.

The waveform of $\tilde{v}$ for several conditions is presented in figure 9. Substantial smoothing of the voltage waveforms was performed before the requisite subtraction. Three results are evident here, as in all $\tilde{v}$ results obtained: (i) $\tilde{v}$ is much more nearly sinusoidal than is the corresponding $\tilde{u}$ fluctuation. (ii) The amplitude of $\tilde{v}$ decreases more rapidly with c/u_∞ than does that of $\tilde{u}$. (iii) The amplitude of $\tilde{v}$ decreases with y less rapidly than does that of $\tilde{u}$.

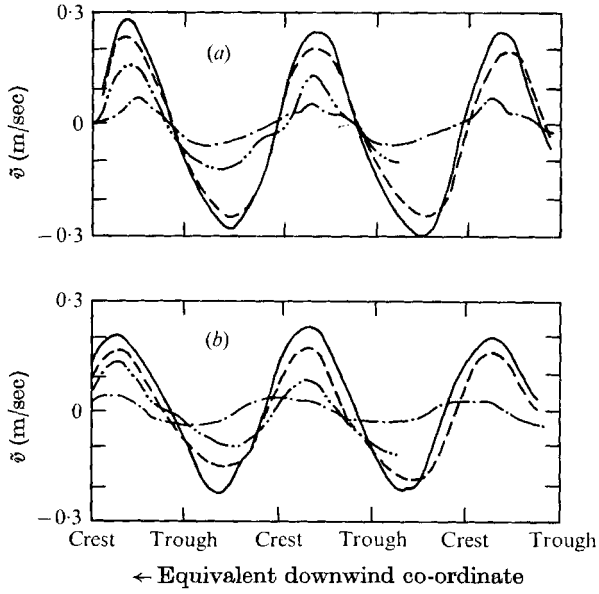

FIGURE 9. $\tilde{v}$ fluctuation, $u_\infty = 5{\cdot}5$ m/sec: (*a*) $y_c = 0{\cdot}060$ in. above crest; (*b*) $y_c = 0{\cdot}240$ in. above crest; ——, – – –, —··—, —·—, $c = 0{\cdot}6$, 1·2, 2·0, 3·0 m/sec, respectively.

Stewart (1967) has called particular attention to the magnitude of $\tilde{v}$ and to its low value over the sea surface. The present measurements indicate values consistent with simple ideas for small c/u_∞. For that case, the peak value of $\tilde{v}$ near the wall should be of the order of $ka[u(y)-c]$, assuming that the streamlines follow the wall. The values appearing in figure 9 for the lowest wave speed are 0·6 and 0·4 $ka[u(y)-c]$ for the two heights. Thus expectation is met. On the other hand, the present measurements also indicate that as c/u_1 assumes values typical of the sea, i.e. of the order of 3–10, the vertical fluctuation becomes much less than the horizontal one, accounting for the difficulty in its detection. The ratio of the peak-to-peak values of the concurrently obtained $\tilde{u}$ and $\tilde{v}$ waveforms, given in figure 10, summarizes this result.

(*d*) *uv correlations.* The correlations $\langle u'v' \rangle$, $\langle \tilde{u}\tilde{v} \rangle$ and $\langle u_t' v_t' \rangle$ were measured for several heights above the wall and for several positive wave-to-wind speed ratios. The $\tilde{u}\tilde{v}$ results, like the $\tilde{v}$ results, were found to be dependent upon the x station of the probe in respect to the ribs of the wall. Again the variation was greatest at the highest values of c/u_∞, and was unimportant for $c/u_\infty \lesssim 0{\cdot}3$. The measurements discussed here were obtained at an x station where $\tilde{u}\tilde{v}$ assumed an average value.

By way of example, figure 11 shows the simultaneous variation of all three correlations at one height and one wave speed. The results are given in the form of a stress coefficient, i.e. $-\rho\langle u'v'\rangle/\frac{1}{2}\rho u_\infty^2$, etc. Note that the correlation $-\rho\langle\tilde{u}\tilde{v}\rangle$ is not a stress until it is averaged. The data points of the figure represent the intervals at which the voltage waveforms were analyzed. The two results for $\langle u_t'v_t'\rangle$ were obtained by the separate techniques described earlier. The result obtained according to $\langle u_t'v_t'\rangle = \langle u'v'\rangle - \langle\tilde{u}\tilde{v}\rangle$ is regarded as being the less accurate of the two.

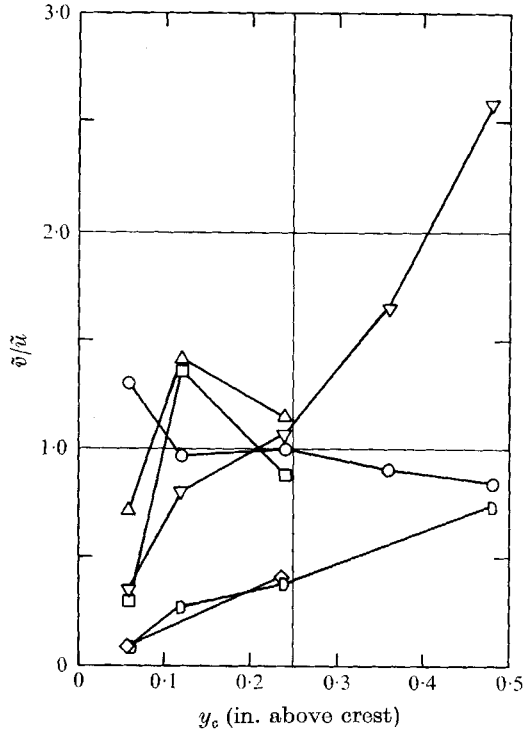

FIGURE 10. Ratio of peak-to-peak values of $\tilde{v}$ and $\tilde{u}$ fluctuations. ○, △, □, ▽, ◇, ▷, c/u_∞ = 0·11, 0·22, 0·36, 0·38, 0·55, 0·64, respectively.

The $\tilde{u}\tilde{v}$ correlation and its corresponding stress do not conform to expectations based upon the inviscid theory in at least two respects. First, the waveform of $-\langle\tilde{u}\tilde{v}\rangle$ in figure 11, as in all other cases, is rather complex, in contrast to the double frequency sinusoid to which the theoretical result is confined. Secondly, it is evident in this case that the average value of that quantity, the stress, is negative, whereas the theory predicts only positive values. The general variation of the stress with height and wave speed is shown in figure 12. The results indicate that although the stress tends toward positive values near the wall, no particular value that can be identified with the pressure drag of the wall is reached. This is not a firm discredit to the theory, however, because the critical layer does not lie entirely outside the innermost measurement height even at the highest c/u_∞. Moreover, the experiment is least accurate at high c/u_∞ on account of wall profile distortion. It is clear that an experiment with waves of smaller amplitude

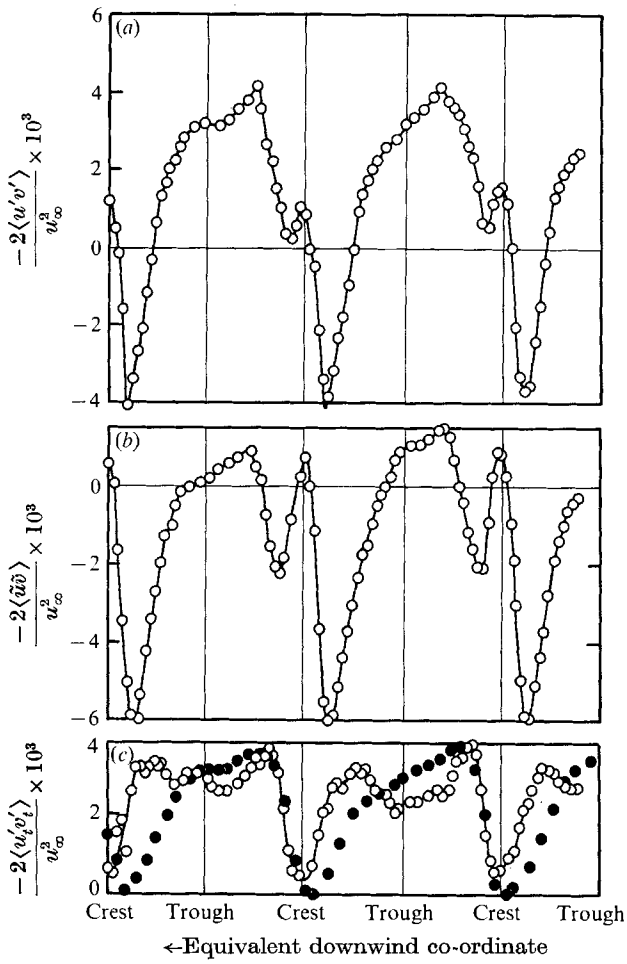

FIGURE 11. uv correlations, $u_\infty = 5{\cdot}5$ m/sec, $c = 1{\cdot}2$ m/sec, $y_c = 0{\cdot}060$ in. above crest: (*a*) total fluctuations; (*b*) repetitive fluctuations only; (*c*) turbulent fluctuations only. Open symbols are difference of curves (*a*) and (*b*).

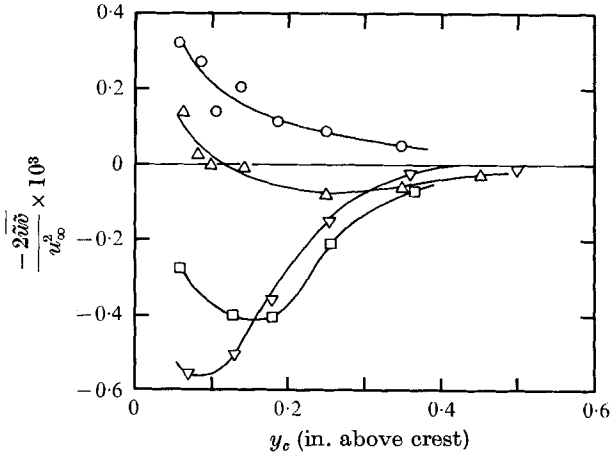

FIGURE 12. $-\tilde{u}\tilde{v}$ stress correlation, $c = 3{\cdot}0$ m/sec: ○, △, □, ▽, $u_\infty = 4{\cdot}7$, 5·5, 6·8, 8·0 m/sec respectively.

and greater spectral purity would be beneficial in examining the region inside the critical layer.

The variation of the turbulent component of the stress with height and with wave speed is shown in figure 13. Two results are apparent. First, the cyclic variation of the stress at a fixed height above the mean surface level is not such that it can be accounted for by the variable distance of the wall below the probe; the stress is not simply dependent upon the height above the instantaneous wave surface. Second, the phase of the cyclic stress variation is shifted upwind with increasing c/u_∞ similarly to that of the turbulent intensity described later.

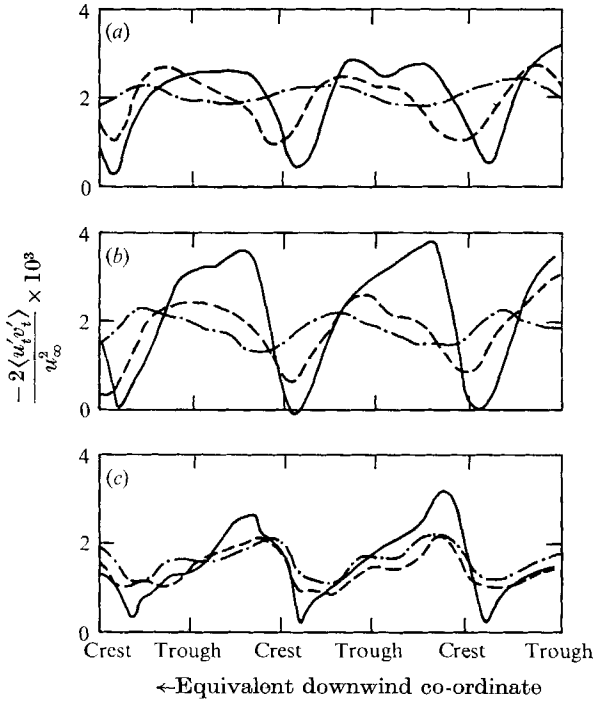

FIGURE 13. Turbulent component of Reynolds stress, $u_\infty = 5{\cdot}5$ m/sec: ——, – – –, —·—, $y_c = 0{\cdot}06$, $0{\cdot}120$, $0{\cdot}240$ in. respectively above crest; (*a*) $c = 0{\cdot}6$ m/sec; (*b*) $c = 1{\cdot}2$ m/sec; (*c*) $c = 3{\cdot}0$ m/sec.

The cyclic variation of $\langle u_t' v_t' \rangle$ and the low value of that quantity attained above the wave crests could be due to a variation of either u_t' or v_t', or to a variation of the correlation between those. The matter cannot be resolved by the measurements obtained in this experiment because the use of a single inclined-wire probe does not enable the measurement of v_t'. The following considerations imply that the correlation coefficient is more variable than the fluctuation intensity. The intensity $\langle c_1^2 u_t'^2 + c_2^2 v_t'^2 \rangle$, where c_1 and c_2 are the hot wire sensitivities is determined as a by-product of the $\langle u_t' v_t' \rangle$ measurements. This intensity is found to exhibit a cyclic pattern whose form and phase resemble those of the $\langle u_t'^2 \rangle$ measurements obtained by the wall probe, described later, even though the paths traced out by the probes differ. For the case shown in figure 11, the ratio

of the maximum to minimum values of $\langle c_1^2 u_t'^2 + c_2^2 v_t'^2 \rangle$ along the cycle is 1·9, or roughly the same as that for $\langle u_t'^2 \rangle$. Simultaneously, the ratio of

$$\langle c_1 c_2 (u_t' v_t') / (c_1^2 u_t^2 + c_2 v_t^2) \rangle,$$

where $c_2 = 1{\cdot}3c_1$, varies between about zero and 0·25. It is virtually certain that the correlation between u_t' and v_t' is quite variable. This may be explained in part by the dependence of the correlation upon the rate of shearing strain $\partial\tilde{u}/\partial y + \partial\tilde{v}/\partial x$. According to figure 6, the strain rate varies by a factor of 10 or more along the wave cycle at a height of, say, 0·1 in. It is minimum a little ahead of the crest, i.e. where $\langle u_t' v_t' \rangle$ is minimum at small c/u_∞.

u_t' intensity and spectra

The turbulent fluctuation intensity $\langle u_t'^2 \rangle$ obtained by means of the wall probe for three wave speeds is shown in figure 14. Two observations may be noted. First, the intensity varies cyclically about an average value approximately

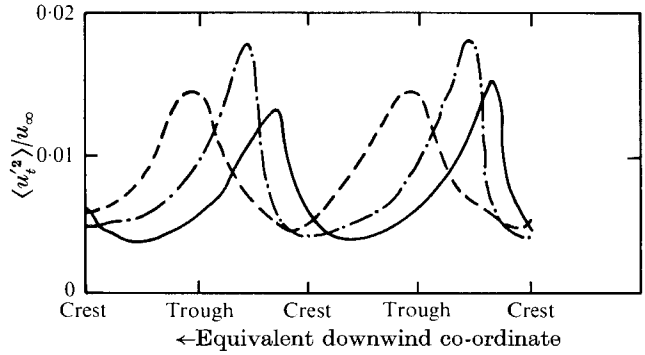

FIGURE 14. Turbulent fluctuation intensity, $u_\infty = 5{\cdot}5$ m/sec, $y = 0{\cdot}120$ in. above wall: ——, —.—, – – –, $c = 1{\cdot}2$, 0·3, $-1{\cdot}2$ m/sec, respectively.

equal to that occurring in a constant-pressure boundary layer, 0·01. Secondly, the phase of the pattern moves upwind as the wave speed increases. The turbulence is 'left behind'. There is an important consequence of these two. Phillips (1966) shows that the normal Reynolds stress results in a force on the wave $F_{uu} = -\rho \overline{\langle u_t'^2 \rangle_0 \partial\zeta/\partial x}$, where the subscript 0 denotes the edge of the sublayer, and ζ is the surface elevation. For the three cases shown in figure 14, the values of $F_{uu} \times 10^3 / \frac{1}{2}\rho u_\infty^2$ are $-0{\cdot}3$, 0·7 and 0·8 for the wave speeds $c/u_\infty = -0{\cdot}22$, 0·05 and 0·22, respectively.

Examination of the cyclic variation of several spectral components of the u_t' fluctuation was carried out at $c = 0$, $u_\infty = 5{\cdot}5$ m/sec and probe height $y = 0{\cdot}12$ in. The results showed that for wave-numbers $k_f = 2\pi f/u_\infty$ below about 2 cm^{-1}, where f is the circular frequency, the variation of the energy of those components resembled that of the total intensity. For $k_f \simeq 4$ cm^{-1}, there was little variation, and for k_f above about 6 cm^{-1}, the variation was in exact opposition to that at low k_f. Spectra $E(k_f)$ were recorded at the two wave stations where the high and the low k_f components assumed extreme values, 15° upwind and 125° downwind

of the crest. Note that the total intensity and that of the low k_f components, is largest where the mean wind speed is least, and *vice versa*. Neither spectrum displayed remarkable features. It was determined that the dissipation parameter $\int_0^\infty k_f^2 E(k_f)\,dk_f$ was nearly equal at the two stations, whereas the integral scale $\frac{1}{2}\pi E(0)$ was 3·6 cm where the intensity was largest, and 6·6 cm where it was least.

Wall stress

The wall stress measurements are necessarily qualitative for a number of reasons. The principal ones are (i) calibration of the stress meter was carried out in an untested environment, (ii) the calibration constants might have been altered during the transfer of the meter from the calibration site to the wavy wall, (iii) such

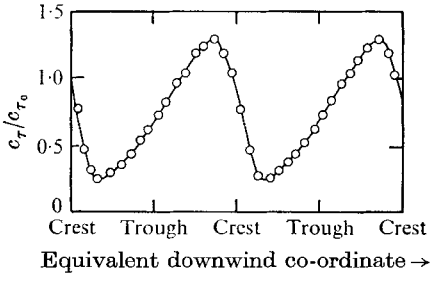

FIGURE 15. Wall shear stress, $u_\infty = 5{\cdot}5$ m/sec, $c = 0$.

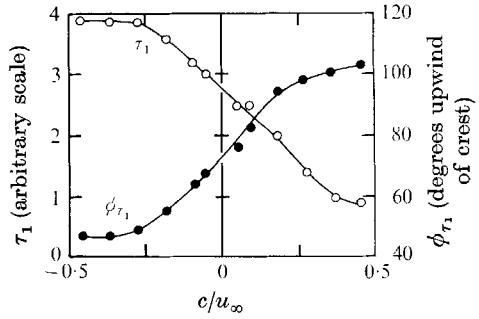

FIGURE 16. Amplitude (open symbols) and phase (solid symbols) of fundamental frequency component of wall shear stress, $u_\infty = 5{\cdot}5$ m/sec.

meters customarily exhibit a difference between the a.c. and d.c. sensitivities owing to the thermal time constant of the substrate, (iv) the meter does not distinguish the sign of the stress. Thus when the turbulent fluctuation of the stress becomes comparable with the average value, considerable error results from the rectification process.

With due caution thus expressed, the ratio of the stress coefficient on the wall to that at the calibration site at the same u_∞ is presented in figure 15. The reference stress, C_{τ_0} is expected to be 0·004. The variation of the amplitude and of the phase of the fundamental frequency component of the stress with c/u_∞ is shown in figure 16. Note that for $c = 0$, the stress phase is about 70° upwind of the crest. The theoretical value given by Benjamin (1959) is 30°.

Summary of phase variation with wind speed

One of the principal results of this experiment is that the phase of the fundamental frequency component of several of the flow perturbation quantities varies with wave speed. Because the value of the phase variation near $c = 0$ may constitute a convenient test of theory, the results are summarized here. The values for $\langle u_i' v_i' \rangle$ and $\langle u_i'^2 \rangle$ are less accurate than for the other quantities.

4. Discussion

The findings of this experiment which bear upon the wave generation process are: (i) There exists an out-of-phase component of the pressure, and therefore a pressure drag. This drag is not due to flow separation, and it is shown that separation is ever less likely to occur as the wave speed increases because the pressure perturbation declines and the wall stress becomes less cyclic. Conversely, it is expected that separation would occur at some upwind wave speed because the average tangential stress is set by the dynamic pressure of the stream, whereas the pressure perturbation increases without limit as c becomes more negative.

Quantity	$\frac{\partial\phi}{\partial c/u_\infty}$, radians
C_{p_1}	+1·2
$\tilde{u}$, wall probe	0
$\langle u_t' v_t' \rangle$	−3
$\langle u_t'^2 \rangle$	−4
C_τ	−1·9

TABLE 4

The present experiments do not, of course, indicate whether separation occurs on sharp-crested water waves. Moreover, the range of Reynolds number tested was inadequate to indicate whether the pressure drag of sinusoidal waves retains a magnitude at high Reynolds numbers sufficient to account for sea wave growth rates. (ii) The contribution of the sinusoidal component of the shear stress to the wave drag may be estimated. Longuet-Higgins (1969) shows the equivalent pressure to be $\delta p = i\tau$; the pressure equals the stress, but is displaced upwind $\frac{1}{2}\pi$. The results of figures 15 and 16 for $c = 0$ show that if the stress observed here prevailed over water waves as well, the incremental drag would be of the order of 3 % of the pressure drag. For $c/u_\infty \simeq 0{\cdot}2$, the incremental drag would vanish, and for $c/u_\infty \lesssim 0{\cdot}2$, would assume negative values.

The linearity of the flow studied in this experiment is important in interpreting the various results. Because only one wave amplitude was tested, the matter cannot be resolved directly. If only the pressure oscillation were considered, then it is likely that the entire range from complete linearity to full non-linearity was encountered here, depending on the wave speed. The experiments of Motzfeld (1937) showed that at $c = 0$, doubling the wave amplitude nearly doubled the pressure, without affecting the pressure phase. Since the amplitude in this experiment was but slightly greater than that of Motzfeld's smaller wave, the pressure here at $c = 0$ would probably have been linear in amplitude. But since only a small upstream progression speed is needed to double the pressure, it is certain that non-linearity ensues at some negative wave speed. If one accepts a non-sinusoidal flow perturbation wave-form as evidence of non-linearity, then the quantities $\tilde{u}$, $\tilde{u}\tilde{v}$, $\langle u_t' v_t' \rangle$ and $\langle u_t'^2 \rangle$ indicate that the flow is not linear under any condition tested.

An attempt to evaluate the adequacy of the inviscid theory leads to ambiguous results. To the apparent credit of the theory, figure 5 showed that the theory predicted the pressure amplitude adequately, and gave the right trend for the phase angle, erring by a relatively constant amount which could be accounted for in some manner. The trend of the $-\overline{\tilde{u}\tilde{v}}$ distribution, figure 12, was partially correct in that at the higher values of c/u_∞, $-\overline{\tilde{u}\tilde{v}}$ became ever larger as the average location of the critical layer was approached from outside. On the other hand, the $\tilde{u}$ oscillations failed to indicate the presence of the predicted vortex above the crests. More importantly, because the inviscid mechanism relies upon the velocity profile curvature, the pressure drag should decline markedly as the critical layer is lowered into the laminar sublayer by a reduction of wave speed. Such was not observed, indicating an altogether different cause of the pressure drag.

The experiments show that the waves strongly modulate the turbulent structure. The two turbulence terms of Phillips' (1966) expression for the wave force, $F_t = -\rho\langle u_t'^2\rangle_0\langle\partial\zeta/\partial x\rangle + \rho(\langle\xi\rangle\partial\langle u_t'v_t'\rangle/\partial y)_0$, are probably important. The first has already been evaluated approximately in §3; the second cannot be evaluated because the probe by which $u_t'v_t'$ is obtained cannot follow the waves. However, for the two lower wave speeds shown in figure 13, the vertical gradients of $u_t'v_t'$ are sizeable, and appear to be in such phase with the wall that the term is positive. The measurements also showed that because the $u_t'v_t'$ stress is so strongly cyclic along the wave, it cannot be represented as a function of distance above the instantaneous surface. Note was made that $u_t'v_t'$ appeared to vary in response to the rate of shearing strain. Because only the amplitude, and not the form or phase, of the strain-producing $\tilde{u}$ and $\tilde{v}$ oscillations changes with wave speed, it would seem appropriate to incorporate a stress perturbation which is proportional to the strain perturbation within a linear theory, as has been done by Reynolds (1968). However, the measurements also show by a phase shift of the cyclic patterns that the turbulent structure lags when the wave speed is varied. It is therefore likely that an intrinsic time constant is an important feature of the flow. This time constant might scale with the ratio of the layer thickness and free-stream velocity for boundary-layer flows, or with the integral scale of the fluctuations and the reference velocity u_1 for logarithmic profile flows of infinite extent. The present measurements deserve further study in an attempt to relate the time constant to the processes of diffusion, dissipation, and rate of change of fluctuation correlation.

This paper presents results of one phase of research carried out at the Jet Propulsion Laboratory, California Institute of Technology, under contract no. NAS7-100, sponsored by the National Aeronautics and Space Administration.

REFERENCES

BENJAMIN, T. B. 1959 *J. Fluid Mech.* **6**, 161.

KARAKI, S. & HSU, E. Y. 1968 *Tech. Rep.* 88, *Dept. of Civil Engineering, Stanford University.*

LIGHTHILL, M. J. 1962 *J. Fluid Mech.* **14**, 385.

LONGUET-HIGGINS, M. S. 1969 *Phys. Fluids*, **12**, 737.

MILES, J. W. 1957 *J. Fluid Mech.* **3**, 185.

MILES, J. W. 1959 *J. Fluid Mech.* **6**, 568.

MOTZFELD, H. 1937 *Z. Angew. Math. Mech.* **17**, 193.

PHILLIPS, O. M. 1966 *The Dynamics of the Upper Ocean.* Cambridge University Press.

REYNOLDS, W. C. 1968 The mechanics of an organized wave in a turbulent shear flow (unpublished). Dept. of Mech. Engineering, Stanford University.

STEWART, R. H. 1969 Ph.D. dissertation, University of California, San Diego.

STEWART, R. W. 1967 *Phys. Fluids Suppl.* **10**, S47.